Solar FTIR measurements of NO$_x$ vertical distributions: Part I) First observational evidence for a seasonal variation in the diurnal increasing rates of stratospheric NO$_2$ and NO

Pinchas Nürnberg[1], Markus Rettinger[1], and Ralf Sussmann[1]

[1]Karlsruhe Institute of Technology, IMK-IFU, Garmisch-Partenkirchen, Germany

Correspondence to: Pinchas Nürnberg (pinchas.nuernberg@kit.edu)

Abstract

Observations of nitrogen dioxide (NO_2) and nitrogen oxide (NO) in the stratosphere are relevant to understand long-term changes and variabilities in stratospheric nitrogen oxide (NO_x) and ozone (O_3) concentrations. Due to the versatile role of NO_2 and NO in stratospheric O_3 photochemistry they are important for recovery and build-up of O_3 holes in the stratosphere, and therefore can indirectly affect the human life. Thus, we present in this work the evaluation of NO_2 and NO stratospheric partial columns (> 16 km altitude) retrieved from ground-based Fourier-transform infrared (FTIR) measurements from over 25 years at Zugspitze (47.42° N, 10.98° E, 2964 m a.s.l.) and 18 years at Garmisch (47.47° N, 11.06° E, 745 m a.s.l.), Germany. The obtained stratospheric columns are only weakly influenced by tropospheric pollution and show only a very small bias of (2.5 ± 0.2) % when comparing NO_2 above Zugspitze and Garmisch. Stratospheric columns of both NO_2 and NO show a diurnal increase in dependence of local solar time (LST). We quantified this behavior by calculating diurnal increasing rates. Here, we find mean values for the NO_2 diurnal increasing rate of $(0.89\pm0.14)\cdot10^{14}$ cm^{-2} h^{-1} and $(0.94\pm0.14)\cdot10^{14}$ cm^{-2} h^{-1} at Zugspitze and Garmisch, respectively. The mean NO a.m. diurnal increasing rate above Zugspitze can be found to be $(1.42\pm0.12)\cdot10^{14}$ cm^{-2} h^{-1}. Regarding the seasonal dependency of these increasing rates, for the first time, we were able to detect a significant seasonal variation of both NO_2 diurnal increasing rates and NO a.m. diurnal increasing rates experimentally with a maximum of $(1.13\pm0.04)\cdot10^{14}$ cm^{-1} h^{-1} for NO_2 and $(1.76\pm0.25)\cdot10^{14}$ cm^{-1} h^{-1} for NO in September and a minimum of $(0.71\pm0.18)\cdot10^{14}$ cm^{-1} h^{-1} in December for NO_2 and a minimum of $(1.18\pm0.41)\cdot10^{14}$ cm^{-1} h^{-1} in November for NO. This similar behavior may be explained by the interconnection of both species in stratospheric photochemistry. The outcome of this work is a retrieval and analyzation strategy of FTIR data for NO_x stratospheric columns, which can help to further validate photochemical models or improve satellite validations. The first use of this data set is shown in a companion paper (Nürnberg et al., 2023) extracting experiment-based NO_x scaling factors describing the diurnal increase out of the retrieved partial columns and validating recently published model-based scaling factors.

1 Introduction

30 Reactive nitrogen oxides (NO_x) as nitrogen monoxide (NO) and nitrogen dioxide (NO_2) play a crucial role in atmospheric photochemistry both in the troposphere and in the stratosphere (Crutzen, 1970). In the tropospheric boundary layer, the NO_x origin is mainly anthropogenic from the combustion of fuels and the use of nitrogen-based fertilizers. To a lower extent, biomass burning and biological processes in soils contribute to NO_x production (Crutzen, 1979). In the upper troposphere near the tropopause, NO_x concentration is mainly controlled by lightning events and air traffic (Grewe et al., 2001). As a precursor

35 for several harmful air pollutants, e.g. ozone (O_3) and nitric acid (HNO_3), the build-upbuilding of NO_x in the troposphere directly affects human health (World Health Organization. Regional Office for Europe, 2003). In the stratosphere, NO_x is produced by the photolysis of nitrous oxide (N_2O), which was transported through the tropopause and is a part of the biospheric nitrogen cycle (Johnston, 1992). As an important part of the O_3-destroying catalytic cycle, NO_x controls the abundance of O_3 in the stratosphere (Murphy et al., 1993). Consequently, since the Montreal Protocol was passed in 1987 with the aim to protect

40 the stratospheric O_3 layer, the monitoring of both O_3 and NO_x became the focus of attention of much research (Tripp, 1987). The global distributions of atmospheric NO_2 and NO have been monitored by satellite missions since 1967 in various operational modes (Godin-Beekmann, 2010; Rusch, 1973): NO_x data products are available from nadir-looking instruments like TROPOMI, GOME and SCIAMACHY (Griffin et al., 2019; Richter and Burrows, 2002; Sierk et al., 2006), limb-viewing instruments like MIPAS and OSIRIS (Funke et al., 2005; Haley et al., 2004) and from solar occultation measurements namely

45 ACE-FTS and SAGE III/ISS (Fussen et al., 2005; Chu et al., 2002). The validation and correction of these data with ground-based measurements is still an ongoing process which significantly reduced statistical and systematic errors between different satellite and ground-based measurements in the past decades (Van Geffen et al., 2022; Verhoelst et al., 2021; Kerzenmacher et al., 2008; Wetzel et al., 2007; Brohede et al., 2007; Heue et al., 2005). However, in comparing data (satellite vs. ground) which are in general recorded during different times of the day a major problem arises: There is a strong diurnal variation of

50 stratospheric NO_x due to a complex photochemistry (Solomon et al., 1986), so biases arise just due to time mismatch.
Facing this mismatch, a common method is the use of correction factors calculated from photochemical models to extrapolate retrieved data to the same time of the day. By now these models have a high accuracy giving information about NO_x concentration in dependence of altitude, latitude and time of the day (Dubé et al., 2020; Strode et al., 2022). However, to the best knowledge of the authors, a reliable analysis of long-term observations of NO_x stratospheric partial columns and their

55 diurnal variations, which could be used for validation of model data, does not exist. This is due to the lack of measurements able to record stratospheric NO_x as function of the time of a day.
For the ground-based observation of NO_x several different measurement techniques are well established such as microwave radiometers (MR), zenith sky (ZS) and multi axis (MAX) differential optical absorption spectroscopy (DOAS) and Fourier-transform infrared (FTIR) spectroscopy. The MR technique is sensitive at high altitudes and offers the possibility to obtain

60 NO_2 columns independent of night- and daytime (Ricaud et al., 2004). ZS-DOAS or Système d'Analyse par Observations Zénithales (SAOZ) instruments are well established at many stations all over the globe, and provide long-term information about trace gas columns (e.g. NO_2) in the stratosphere (Platt and Stutz, 2008; Vandaele et al., 2005; Pommereau and Goutail, 1988; Solomon et al., 1987). However, these instruments especially have a good sensitivity at high SZA near sunrise or sunset (Tack et al., 2015). To get information at lowerhigh SZA, MAX-DOAS measurements are performed providing information

65 about tropospheric trace gas concentrations at different times of the day (Dimitropoulou et al., 2020; Hönninger et al., 2004). However, these measurements do not provide information about trace gas concentrations atnear the tropopause and in the lower stratosphere.
Accurate information on NO_2 and NO columns are accessible via FTIR solar absorption spectrometry, which can cover the whole diurnal variation of NO_x (Fischer, 1993). Since the first ground-based FTIR measurements of NO_2 (Camy-Peyret et al.,

70 1983) and NO (Hanst et al., 1982), some effort was made in monitoring seasonal trends and diurnal variation of stratospheric and tropospheric NO_x (Zhou et al., 2021; Yin et al., 2019; Virolainen et al., 2014; Hendrick et al., 2012; Flaud et al., 1988;

Rinsland et al., 1988). However, the multitude of this research investigated time periods covering only a few days up to several months. An examination of reliable long-term FTIR measurements with regard to stratospheric NO_2 columns was done by Hendrick et al. (2012). Even though the NO_2 diurnal variation is not discussed, the evaluation of 20 years of measurements above Jungfraujoch depict a consistent picture of 1) the seasonal variability of stratospheric NO_2 columns which undergoes a maximum in summer and a minimum in winter and 2) a long-term trend which seems to show a slight decrease of stratospheric NO_2 in the order of 3.6 % over 20 years from 1990 - 2010. Already before, a study of Sussmann et al. (2005) had quantified the NO_2 diurnal variation from ground-based FTIR measurements at the Zugspitze. This study successfully showed, that the stratospheric NO_2 diurnal variation can be measured at a high-altitude site without the strong influence of tropospheric pollution events (Sussmann et al., 2005). However, due to the comparably short time period analyzed in this earlier study (2.5 years), a seasonal dependency could not be retrieved. Another reliable long-term study from Zhou et al. (2021) analyzed NO tropospheric and stratospheric partial columns retrieved from FTIR measurements above Xianghe and Maido. This study comprises both the seasonal variability of stratospheric NO with a maximum in winter and a minimum in summer and the diurnal variation of it in dependence of the local time (Zhou et al., 2021). However, a quantification regarding the seasonal dependence of the diurnal increase was not discussed.

Therefore the goal of this work is i) to analyze the full Zugspitze and Garmisch FTIR time series covering more than 25 years (1995-2022) and 18 years (2004-2022) of measurements, respectively, to derive the slope of the linear fit diurnal increase of NO_2 and NO stratospheric columns in dependence of the local solar time (LST) - namely the diurnal increase - above our mid-latitude sites while eliminating the impact of tropospheric pollution or tropopause variabilities, ii) investigate whether a significant seasonal variation of the NO_2 diurnal increase can be inferred, and iii) perform a comparison to NO stratospheric columns to further validate the analyzation method and the reliability of the obtained data. The measurement data set published along with this paper will be a solidsound basis for validating current and upcoming photochemistry model simulations and improving satellite validation.

This paper is Part 1 of two companion papers dealing with the experimental description of the diurnal NO_x variability above Zugspitze by means of ground-based FTIR measurements. Our paper will first discuss the stratospheric NO_x photochemistry and the consequences for the diurnal behavior of NO_2 and NO in Sect. 2. In Sect. 3 we will describe the retrieval strategy for NO_2 and NO from solar FTIR measurements at Zugspitze and Garmisch. Section 4 will focus on the retrieval results, the separation of the retrieved columns into stratospheric and tropospheric contributions, and the introduction of a pollution filter for the obtained stratospheric columns. The calculation of NO_2 diurnal increasing rates and their seasonal variation will be made in Sect. 5 followed by a comparison to NO a.m. diurnal increasing rates validating the analyzation method in Sect. 6. Section 7 gives the summary and conclusions.

2 Photochemistry of stratospheric NO_x

As a background for our later FTIR-data interpretation, we ~~thereafter~~ present a short overview of~~over~~ the model understanding

105   of NO_x stratospheric photochemistry. More details can be found in the literature (Crutzen, 1970; Crutzen, 1979; Coffey et al., 1981; Cariolle, 1983; Jaeglé et al., 1994; Lary, 1997; Cohen and Murphy, 2003; Brasseur and Solomon, 2005).

During daytime the main NO_2 source is the photolysis of the reservoir species HNO_3 and N_2O_5, see Eq. (R1) and (R2), resulting in a continuous~~consecutive~~ increase of NO_2 within the day.

$$HNO_3 + hv \rightarrow NO_2 + OH, \tag{R1}$$

110   $$N_2O_5 + hv \rightarrow NO_2 + NO_3. \tag{R2}$$
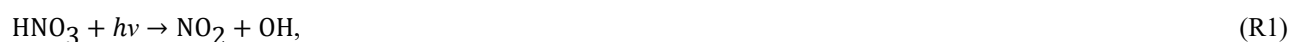
Both reactions take place on a time scale of minutes to hours between sunrise and sunset and the kinetics depend on solar elevation.

The main NO source is the reaction of nitrous oxide (N_2O) with excited~~exited~~ oxygen ($O(^1D)$) resulting from the photolysis of O_3 given in Eq. (R3) and (R4). This leads to a similar continuous~~consecutive~~ increase of NO within the day as seen for NO_2.

115   $$O_3 + hv \rightarrow O(^1D) + O_2, \tag{R3}$$

$$N_2O + O(^1D) \rightarrow 2\ NO. \tag{R4}$$

According to the model understanding, the reaction rate of Eq. (R1) to (R4) decreases after noon leading to a lower NO_2 and NO increase in the afternoon than observed in the morning.

Additionally, both NO_x species are interconverted into each other ~~very fast~~ on time scales of seconds within the O_3-destroying

120   nitrogen catalytic cycle

$$NO + O_3 \rightarrow NO_2 + O_2, \tag{R5}$$

$$NO_2 + O \rightarrow NO +\ O_2, \tag{R6}$$

$$net: O\ +\ O_3 \rightarrow 2\ O_2, \tag{R7}$$
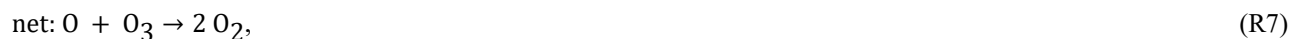
and via the photolysis of NO_2 (Eq. (R8)), resulting in an equilibrium during daytime.

125   $$NO_2\ +\ hv \rightarrow NO +\ O. \tag{R8}$$

This equilibrium is reached very fast after sunrise and is nearly constant in the morning where the concentration increase of both species follows in a good approximation a linear behavior. In the afternoon, the equilibrium is changing due to the strong solar elevation dependency of Eq. (R8) and due to the increasing abundancy of O_3 with daylight~~daytime~~ (Wang et al., 2020; Strode et al., 2022). Consequently, after noon, the NO increase slows down, whereas NO_2 continues to increase with a similar

130   rate.~~.~~ Between SZA = 80°-90° the trace gas concentrations are still influenced by the thermally driven reactions taking place at night, leading to a strong deviation from a linear behavior during very early morning.

3 FTIR measurement and retrieval strategy

3.1 Measurement

All data of this study are retrieved from long-term ground-based FTIR solar absorption measurements at the Zugspitze,

135   Germany (47.42° N, 10.98° E, 2964 m a.s.l.) and Garmisch, Germany (47.47° N, 11.06° E, 745 m a.s.l.). The high-altitude observatory at Zugspitze is located in the German alps and can be treated as a clean site without strong influences from pollution events in the boundary layer. The observatory at Garmisch is located in direct vicinity to the Zugspitze, but 2219 m below in the countryside under the influence of urban pollution events from e.g. Munich. The used Bruker IFS 125HR spectrometers are operated continuously since 1995 at the Zugspitze and since 2004 at Garmisch. They operate with an actively

140   controlled solar tracker and liquid-nitrogen cooled MCT (HgCdTe) and InSb detectors. Instrument and measurement details are described elsewhere in detail (Sussmann and Schäfer, 1997; Sussmann, 1999). The used data set for the Zugspitze comprises all available measurements since 1995 to now. Namely 19,552 spectra on 2,579 measurement days (7.58

measurements per measurement day on average) for the micro-window (MW) used for the NO_2 retrieval and 7,513 spectra on 2,247 measurement days (3.34 measurements per measurement day on average) for the NO retrieval. The maximum optical path difference is 175 cm and 250 cm, respectively. The used data set for Garmisch comprises all available measurements since 2004 to now. Namely 15,801 spectra on 2,114 measurement days (7.47 measurements per measurement day on average) for the MW used for the NO_2 retrieval.

3.2 Retrieval strategy

In this paper, NO_2 and NO volume mixing ratio (VMR) profiles and column amounts are derived from measured spectra using version 9.6 of the retrieval code PROFFIT (Hase et al., 2004). The used parameters of the two described retrievals are summarized in detail in Table S1 in the supplement. They are all optimized leading to minimum values of the resulting spectral residuals (measured minus calculated) and physically meaningful vertical VMR profiles. The main quality selection criterion after a successful retrieval (< 20 iterations) was a ratio of the noise-to-signal ratio (NSR) to the degrees of freedom for signal (DOFS) of $\frac{NSR}{DOFS} \leq 0.125$ for NO_2 and ≤ 0.2 for NO, respectively. These settings have been determined by a tradeoff between data quality and data amount. The DOFS is a measure of the information content that can be attained on the vertical profile from the retrieval (Rodgers, 1998). Additionally, all spectra recorded at SZA > 80° were dropped because of the influence of the thermally driven reactions taking place at night, which can be dominant already near the terminator (SZA = 90°, see Sect. 2). However, this dropped data is available from~~The resulting mean calculated spectra for~~ the corresponding author upon request. The resulting mean calculated spectra for~~NO₂ and~~ the NO_2~~NO retrieval, their spectral residuals,~~ and the NO retrieval, their spectral residuals, and~~NSR are shown in Fig. S1a and b and Fig. S2, respectively. The latter is NSR = 0.0694 % (NO₂) and 0.1603 % (NO) at the~~ NSR are shown in Fig. S1a and b and Fig. S2, respectively. The latter is NSR = 0.0694 % (NO_2) ~~and 0.1603 % (NO) at the~~ Zugspitze and 0.0631 % (NO_2) at Garmisch.

3.2.1 NO_2

For retrieval of NO_2 above the Zugspitze and above Garmisch a prominent infrared absorption line first suggested for atmospheric retrievals by Camy-Peyret et al. (1983) was used, utilizing a spectral MW ranging from 2914.3 cm^{-1} to 2914.85 cm^{-1}. This MW includes a strong absorption of CH_4 at 2914.5 cm^{-1} which is retrieved simultaneously. For both species (NO_2 and CH_4) we applied a simple first-derivative (L_1) smoothness constraint (Tikhonov, 1963). Vertical a priori profiles of the interfering species H_2O, O_3, H_2CO, OCS, and C_2H_6 were iteratively scaled within the retrieval. For NO_2 one single averaged a priori profile was taken from the Whole Atmosphere Community Climate Model (WACCM) version 6 generated by NCAR (Lamarque et al., 2013). Daily profiles from the GGG2020 software (Laughner et al., 2022) were used for the interfering species. The spectroscopy for all species is taken from ATMOS version 20200512 (Brown et al., 1996).

3.2.2 NO

For retrieval of NO above the Zugspitze the prominent doublet located at 1900.075 cm^{-1} was used, utilizing a spectral MW ranging from 1899.900 cm^{-1} to 1900.100 cm^{-1}. This MW was also used in previous studies (Zhou et al., 2021; Wiacek et al., 2006; Notholt et al., 1995). This MW includes an absorption line of CO_2 at 1899.995 cm^{-1} which is retrieved simultaneously. For both species (NO and CO_2) we applied a L_1 Tikhonov regularization. A vertical a priori profile of O_3 was iteratively scaled within the retrieval. For the other interfering species H_2O and N_2O only a forward calculation was used along within retrieval of the other species. For NO one single averaged a priori profile was taken from the Whole Atmosphere Community Climate Model (WACCM) version 6 generated by the NCAR (Lamarque et al., 2013). Daily profiles from the GGG2020 software were used for the interfering species (Laughner et al., 2022). The spectroscopy for all species is taken from HITRAN2020 (Gordon et al., 2022).

4 NO$_x$ vertical profiles and pollution filter

Following the retrieval strategy and the quality control described in Sect. 3, NO$_x$ vertical profiles are derived above Zugspitze (NO$_2$ and NO) and above Garmisch (NO$_2$) for each spectrum and are shown in the supplement material in Fig. S3a (Zugspitze) and b (Garmisch) for NO$_2$ and in Fig. S4a and b for NO (red lines). From the remaining 16,023 (Zugspitze, NO$_2$), 14,460 (Garmisch, NO$_2$) and 6,213 (NO) spectra a mean DOFS of 1.38, 1.49 and 2.14, respectively, are derived.

4.1 Separation of the tropospheric and stratospheric column contributions

As mentioned in the introduction, one main issue of this work is the reduction of error sources influencing the reliability of the interpreted data. To avoid the influence of NO$_x$ variability in the troposphere and near the tropopause on the retrieved stratospheric NO$_x$ columns, in this section we will describe the separation of the derived columns into two partial columns, even though the obtained DOFS for the NO$_2$ retrieval are only 1.38 (Zugspitze) and 1.49 (Garmisch) and not 2.0. The lower partial column covers the troposphere and the lower stratosphere up to 16 km. The upper partial column covers the middle and upper stratosphere above 16 km.

4.1.1 NO$_x$ partial column averaging kernels above Zugspitze and Garmisch

Figure 1a depicts the retrieved number density (mean over all measured spectra) of NO$_2$ as a function of altitude z at Zugspitze (continuous gray line) and Garmisch (broken line) normalized to its maximum value in the stratosphere. Additionally, the partial column averaging kernels (PCK, sum of the rows of the averaging kernel matrix over the respective altitude range of the partial column of interest) for both retrievals below (red line) and above (blue line) 16 km altitude are shown. For both stations, a nearly identical profile (gray) is obtained, confirming the retrieval method. The first local maximum extends over the lower troposphere up to 8 km altitude. This maximum reflects the mainly anthropogenic NO$_x$ sources in the boundary layer. Although the measurements are performed on a high-altitude site (Zugspitze), the influence of anthropogenic NO$_x$ sources from the boundary layer on the profile cannot be excluded. Another contribution certainly results from the a priori profiles (given the shape of the a prioris used as depicted in Fig. S3 (green line) along with the weak sensitivity of the PCK < 16 km (red continuous line) for the 2.964-8 km range). Near the tropopause between 5 km and 15 km another local maximum is visible. This accumulation is typical for mid-latitudes and can be explained by mainly the influence of lightning in summer, the vertical transport of NO$_x$ from surface emissions and air traffic (Grewe et al., 2001). Above 16 km a large peak is apparent in the profiles with a maximum at ~ 30 km. Here, the stratospheric NO$_x$ / O$_3$ photochemistry is taking place which is the focus of this work.

Figure 1b depicts in the same manner the retrieved mean number density for NO normalized to its maximum value in the stratosphere against z (gray line) and the PCK below (red line) and above (blue line) 16 km altitude. The NO profile (gray) shows analogous maxima as described above for NO$_2$. The lowest maximum results from anthropogenic emissions in the boundary layer, the maximum near the tropopause results from lightning events, vertical NO$_x$ transport and air traffic and the maximum at 30 km altitude reflects NO$_x$ / O$_3$ photochemistry in the stratosphere.

To give reason for a separation of the stratospheric columns from the lower ones, the PCK for < 16 km (red lines) and > 16 km (blue lines) altitude are depicted in Fig. 1a and b too.

The lower PCK of the NO$_2$ retrieval at Zugspitze (continuous red line, Fig. 1a) shows a moderate sensitivity in the altitude region between 2.964 km and 16 km with a maximum of 0.38 at 18 km. In contrast, the lower PCK of the NO$_2$ retrieval at Garmisch (dotted red line, Fig. 1a) shows a strong sensitivity in the lower altitude region with a maximum of 1.33 at 17 km. However, for both retrievals the sensitivity of the lower PCK at high altitudes of 30 km is very low with 0.18 and 0.35, respectively. Here, both stratospheric PCK (blue line), which are very similar for the retrieval at Zugspitze (continuous line) and Garmisch (dotted line), show a high retrieval sensitivity of ca. 1 above 30 km and a comparably low sensitivity below 16 km.

For the NO retrieval at Zugspitze (Fig. 1b) a similar pattern is achieved. The sensitivity of the lower PCK (red line) is rather high above the tropopause with a maximum of 0.69 at 18 km but it decreases strongly to higher altitudes (0.11 at 30 km). In comparison, the stratospheric PCK (blue line) as seen for NO_2 shows a continuous high sensitivity to stratospheric variabilities with a value of ~ 1 above 30 km.

These findings make it reasonable to split up the obtained NO_2 and NO profiles into partial columns above and below 16 km altitude to avoid influences of variabilities near the tropopause and in the boundary layer upon the stratospheric partial column, although the resulting DOFS of the NO_2 retrieval are only 1.38 (Zugspitze) and 1.49 (Garmisch).

4.2 Pollution filter

In a next step the obtained NO_x lower partial columns should be used to account for pollution events in the boundary layer which also could affect the data retrieved for the stratospheric partial column and especially their diurnal variability. Figure S5a-d in the supplement show the retrieved NO_2 partial columns above Zugspitze (top row) and above Garmisch (bottom row) below (left) and above (right) 16 km altitude in dependence of ~~local solar time~~ (LST~~)~~ and partitioned into monthly data sets for the whole measurement period (blue to yellow symbols from January to December, see legend). To account for pollution events the evidently visible positive outliers of the lower partial columns (left) are identified via the interquartile range (IQR). All dates on which the retrieved lower partial column is above 1.5·IQR of the respective month are removed from the dataset and, consequently, will not show up in the stratospheric column too. The resulting pollution filtered NO_2 partial columns are shown in Fig. 2 for the measurements at Zugspitze (top row) and Garmisch (bottom row) and will be discussed in the next section. In the same manner we filtered the retrieved NO data set (see Fig. S6 top row (raw data) and bottom row (pollution filtered)) to account for tropospheric pollution events.

4.3 NO_2 partial columns above Zugspitze and Garmisch

In Fig. 2, the pollution filtered NO_2 partial columns below (left) and above (right) 16 km altitude measured at Zugspitze (top row) and Garmisch (bottom row) are shown. In comparison to the uncorrected data, the monthly data sets for both NO_2 partial columns are smooth.~~highly smoothened.~~ In the troposphere and near the tropopause (lower partial column, Figure 2a and c) the NO_2 concentration does not show a diurnal variation in dependence of the LST. This behavior agrees with the literature and underlines the weak influence of photochemistry in the lower atmosphere (Li et al., 2021). Comparing the lower partial column above Zugspitze (Figure 2a) and Garmisch (Figure 2c), the difference in altitude (2219 m) of both observatories is directly visible. Due to the influence of anthropogenic emissions in the boundary layer, the lower partial column measured at Garmisch shows 7-10 times higher values than measured at Zugspitze, see also Fig. S7a in the supplement.

Contrary to this, both stratospheric partial columns (> 16 km) above Zugspitze (Figure 2b) and Garmisch (Figure 2d) have very similar values, see also for a direct comparison Fig. S7b. Due to the vicinity of both observatories (ca. 10 km) it is to be expected that the stratospheric partial columns are practically identical. However, the question is whether the data retrievals can reflect this expectation because of the extremely differing station altitudes, with tropospheric NO_2 potentially impacting the Garmisch stratospheric retrievals more than in the Zugspitze case. When quantitatively comparing both timeseries, the mean bias of both partial columns over the whole period between 2004 and 2022 can be found to be only 2.5 %. The standard error of the bias is lower ($2·\sigma/\sqrt(n) = 0.28$ %), indicating that the 2.5 % difference between the stratospheric NO2 partial columns measured at Zugspitze and Garmisch is small but significant. Anyhow, the very low mean bias between both data sets validates the used retrieval method and confirms the data evaluation up to this point. Additionally, both stratospheric partial columns show a strong diurnal variation with LST. Here, the discussed diurnal increase from sunrise to sunset is well pronounced for every month. The influence of the stratospheric NO_2 seasonal cycle can be seen when comparing the different months (blue to yellow symbols from January to December, see legend). The NO_2 concentration in summer (greenish symbols) is ~3.5 times higher than in winter time (blueish and yellowish symbols) which can be clearly seen when comparing summer

and winter months in Figure 3.). This is in good agreement with long-term literature data from Jungfraujoch, which is a high-altitude site at mid-latitudes (Hendrick et al., 2012).

5 NO₂ diurnal increasing rate

In this section we will use the pollution filtered NO₂ stratospheric partial columns measured at Zugspitze and Garmisch to calculate diurnal increasing rates in dependence of the month. The latter quantitatively describes the seasonal variation in diurnal stratospheric NO₂ concentrations. For validation of the observed behavior and the used retrieval method we will furthermore correlate the obtained NO₂ diurnal increasing rates from both observatories (Zugspitze and Garmisch).

5.1 Calculation of monthly NO₂ diurnal increasing rates

Figure 3 shows the NO₂ stratospheric partial columns measured at Zugspitze (red open symbols) and Garmisch (blue closed symbols) in dependence of the LST for every month. As discussed before, the data of both observatories are very similar when comparing data of the same time of the day. Note that especially in winter, the data range measured at Garmisch is smaller due to the combination of low solar altitude angle and the location of the observatory in the valley, leading to a higher uncertainty of the resulting data in the winter compared to Zugspitze.

Within our observational data scatter, we cannot confirm from Fig. 3 any non-linear behavior of the NO₂ diurnal increase after noon as forecasted from some models (Dubé et al., 2020; Mclinden et al., 2000). Instead, the measured NO₂ column appears to increase linearly over the whole day for every time of the year. One reason for this deviation can be the altitude-dependence of the non-linearity of the NO₂ concentration discussed by Dubé et al. (2021), which cannot be addressed with NO₂ column data available in this work. HoweverConsequently, we decided to extract NO₂ diurnal increasing rates from the observed data by the determination of the slope of a linear fit over the whole day for every month at Zugspitze (black dashed lines) and Garmisch (black dotted lines). A similar method for the determination of NO₂ diurnal increasing rates was applied in earlier work (Sussmann et al., 2005; Li et al., 2021).

The results of the linear fits in dependence of the month are shown in Fig 4a for the measurements at Zugspitze (red open symbols) and Garmisch (blue closed symbols). The calculated mean values are also indicated in the Figure and are $(0.89\pm0.14)\cdot10^{14}$ cm⁻² h⁻¹ and $(0.94\pm0.14)\cdot10^{14}$ cm⁻² h⁻¹ for Zugspitze and Garmisch, respectively. The errors are two times the standard error of the mean $(2\cdot\sigma/\sqrt{n})$, i.e., the mean values agree perfectly within error bars. Both increasing rates also agree within error bars with the value of $(1.02\pm0.12)\cdot10^{14}$ cm⁻² h⁻¹ obtained in our earlier work for Zugspitze (Sussmann et al., 2005), where a smaller data set (only 2 years) and a simpler retrieval approach had been utilized (using a total column retrieval with a zero a priori below 10 km altitude instead of a full profile retrieval). Furthermore, Li et al. (2021) published for an even smaller timespan (only one week in October 2018) a value of $(1.34\pm0.24)\cdot10^{14}$ cm⁻² h⁻¹ for the NO₂ diurnal increasing rate above Table Mountain, California (34.38° N). This value roughly agrees with the values measured in this work for October which are $(0.92\pm0.04)\cdot10^{14}$ cm⁻² h⁻¹ and $(1.01\pm0.05)\cdot10^{14}$ cm⁻² h⁻¹ for Zugspitze and Garmisch, respectively. Here, the even smaller database but also the differing latitude (~13°) could explain the difference.

Besides the discussion of averaged NO₂ diurnal increasing rates and single monthly values, in Fig. 4a a clear seasonal variability of the diurnal increasing rate obtained at Zugspitze and at Garmisch is visible. As reflected by the small error bars of the calculated monthly mean values in Fig. 4a, for both observatories for the first time a seasonal cycle with a maximum of $(1.13\pm0.04)\cdot10^{14}$ cm⁻¹ h⁻¹ in September and a minimum of $(0.71\pm0.18)\cdot10^{14}$ cm⁻¹ h⁻¹ in December can be shown experimentally. For the quantitative validation of this new finding we directly correlate the obtained monthly NO₂ diurnal increasing rates measured at Zugspitze and Garmisch in the next section, expecting both to have the same origin in stratospheric photochemistry and therefore are correlated.

5.1.1 Correlation analysis of extracted diurnal increasing rates

Figure 4b shows the scatter plot of monthly NO_2 diurnal increasing rates measured at Garmisch against the ones measured at Zugspitze. The error bars are $\pm 2 \cdot \sigma$ (standard deviation) from the linear fit. The red continuous line is the linear regression with x- and y-error weighting with the method by York et al. (2004). With the assumption, that x- and y-errors are not correlated, the regression analysis results in the values given in Table 1. Additionally, the regression without error-weighting is shown (red dotted line). Whereas the correlation coefficient r is independent of the errors, the t-value strongly depends on the error. If the t-value exceeds the critical t-value $t_{crit}(95\%) = 2.23$, a significant correlation within 95 % confidence is given. In this case, with a high correlation coefficient $r = 0.7899$ and with a t-value of 3.96 and 3.37 with and without error-weighting, respectively, it is very likely that the data are correlated. This result confirms that the shown seasonal variation of the NO_2 diurnal increasing rates is a real effect, which is probably originated in the stratospheric photochemistry at midlatitudes.

6 NO increasing rate

In this section we will analyze the retrieved NO stratospheric columns above Zugspitze. This analysis~~analyzation~~ is motivated by the question of whether the observed seasonal dependence of the NO_2 diurnal increasing rate originates~~is originated~~ in ~~the~~ stratospheric photochemistry and consequently can be seen in the NO data too.

6.1 Calculation of monthly NO a.m. diurnal increasing rate

Figure 5 shows the ~~dependence of the~~ stratospheric NO partial columns measured at Zugspitze (yellow open symbols) as a function of~~on~~ the LST for every month. Unlike as seen for NO_2, for NO the non-linear behavior of the diurnal increase is well-pronounced and especially in summertime (mid row) after local solar noon the slope of the diurnal increase decreases significantly. As described in Sect. 2, this behavior can be attributed on the one hand to the strong solar elevation dependency of Eq. (R8). On ~~the other hand,~~ the ~~other hand, the~~ increasing abundance~~abundancy~~ of O_3 with daytime influences the kinetics of Eq. (R7). Both effects lead to a change in the chemical equilibrium between NO_2 and NO after local solar noon and explain the different afternoon behavior of both trace gases.

For the quantification of the diurnal increase of the NO stratospheric partial column and a good comparability to NO_2, here~~,~~ we only make a monthly linear fit before noon (Figure 5, black dashed line) to extract a NO a.m. diurnal increasing rate for every month.

The results of the linear fits in dependence of the month are shown in Fig. 6 (yellow open symbols) together with the NO_2 diurnal increasing rates measured at Zugspitze (red open symbols). It can be seen, that the NO a.m. diurnal increasing rate shows a similar seasonal variation as the NO_2 diurnal increasing rate with a maximum of $(1.76\pm0.25)\cdot10^{14}$ cm^{-1} h^{-1} in September and a minimum of $(1.18\pm0.41)\cdot10^{14}$ cm^{-1} h^{-1} in November. Here, a correlation of NO_2 and NO diurnal increasing rates is likely.

However, the error bars of the linear fits of NO are significantly larger compared to NO_2. One main reason beside others for this effect is the smaller data base for the NO retrieval with less than one half of the spectra compared to NO_2 (16,023 vs. 6,213 spectra). This difference originates~~is originated~~ in ~~the~~ use of another MW for the NO retrieval. Nevertheless, in the next section we will make a correlation analysis of both diurnal increasing rates to quantify the relationship between stratospheric NO_2 and NO.

6.1.1 NO₂-NO correlation analysis

In Fig. 6b a scatter plot of monthly NO a.m. diurnal increasing rates against the NO_2 diurnal increasing rates is shown, both measured at Zugspitze. The error bars are $\pm 2 \cdot \sigma$ from the linear fit. The red continuous line is the linear regression with x- and y-error weighting with method of York et al. (2004) as described in the Sect. 5.1.1. The red dotted line represents the fit without weighting. The results of the correlation analysis are given in Table 2.

The high correlation coefficient of $r = 0.7798$ shows, that it is likely that the given data are related. Without considering the error bars, the t-value (3.94) exceeds t_{crit} (2.23) for a confidence level of 95 %, reflecting a significant correlation of the data within 95 % confidence. However, due to the larger error bars of the NO a.m. diurnal increasing rates, the application of error-weighting leads to an even smaller t-value of 0.83, resulting in no statistical correlation of both data sets within 95 % confidence. Nonetheless, we would like to argue, that the obvious similarity between the seasonality of the NO_2 and NO a.m. diurnal increasing rate observed in Fig. 6a is not accidental. If so, this observation would confirm our model understanding of an interconnection of both trace gases in the stratospheric photochemistry.

7 Summary and Conclusions

In this study, we analyzed long-term FTIR data recorded within the last 25 years at Zugspitze (47.42° N, 10.98° E, 2964 m a.s.l.) and Garmisch (47.47° N, 11.06° E, 745 m a.s.l.), Germany. We present a retrieval and analyzation strategy for the given FTIR data, which provides NO_2 and NO stratospheric partial columns (> 16 km altitude) which are only weakly influenced by the tropospheric partial column and by pollution events. The obtained NO_2 stratospheric partial columns are with a bias of only (2.5±0.2) % very similar above Zugspitze and Garmisch, reflecting the reliability of the given analysis. The observed diurnal behavior of both the NO_2 and the NO stratospheric partial columns in dependence of the local solar time (LST) reflects the expected behavior described in the literature via photochemical model simulations: The NO_2 stratospheric partial column follows over the whole day and independent of the season a linear increase from sunrise to sunset. In a similar way, the NO stratospheric partial column increases linearly before local solar noon. In the afternoon, the increase in~~slope of the~~ NO stratospheric partial column slows down~~rise decreases~~ significantly, especially in summertime. Beside these basic observations, we quantified the described diurnal increase of NO_2 and NO in dependence of LST by calculating monthly NO_2 diurnal increasing rates above Zugspitze and Garmisch with mean values of $(0.89\pm0.07)\cdot10^{14}$ cm^{-2} h^{-1} and $(0.94\pm0.07)\cdot10^{14}$ cm^{-2} h^{-1}, respectively and monthly NO a.m. diurnal increasing rates above Zugspitze with a mean value of $(1.42\pm0.06)\cdot10^{14}$ cm^{-2} h^{-1}. Here, the mean NO_2 diurnal increasing rates perfectly fits together with a literature value published by Sussmann et al. (2005). Additionally, for the first time we could show a significant seasonal variation of both the NO_2 diurnal increasing rate and the NO a.m. diurnal increasing rate experimentally with a maximum of $(1.13\pm0.04)\cdot10^{14}$ cm^{-1} h^{-1} for NO_2 and $(1.76\pm0.25)\cdot10^{14}$ cm^{-1} h^{-1} for NO in September and a minimum of $(0.71\pm0.18)\cdot10^{14}$ cm^{-1} h^{-1} in December for NO_2 and a minimum of $(1.18\pm0.41)\cdot10^{14}$ cm^{-1} h^{-1} in November for NO. Although the correlation analysis of both NO_2 and NO diurnal increasing rates give quantitative evidence for their interconnection in the stratospheric photochemistry only within 85 % confidence, both diurnal increasing rates follow the same seasonal cycle.

Part 2 of the companion papers (Nürnberg et al., 2023) will show the generalization of the observed NO_x partial columns (> 16 km) by converting them into experiment-based NO_x scaling factors describing the NO_x diurnal variability in dependence of SZA, and will give a first comparison to recently published model-based scaling factors.

The data and analysis method given in this paper (Part 1) can be the first step for a latitude dependent (multi-station) data set reflecting the diurnal behavior of the stratospheric NO_x column in dependence of season. Furthermore, the measurements with its high time resolution can serve as a basis for the validation of future photochemistry models and the improvement of satellite validation.

Data availability

The data underlying this publication can be obtained at any time from the corresponding author on demand.

380 **Competing Interests**

None.

Acknowledgements

Funding by the Federal Ministery of Education and Research of Germany within the Project ACTRIS-D (grant 01LK2001B) is gratefully acknowledged. We acknowledge funding by the Helmholtz Research Program "Changing Earth – Sustaining our
385 Future" within the Research Feld "Earth and Environment" and by the KIT-Publication Fund of the Karlsruhe Institute of Technology. We would like to thank Sarah A. Strode for carefully reading the manuscript.

References

Brasseur, G. P. and Solomon, S.: Aeronomy of the Middle Atmosphere, 3, Aeronomy of the Middle Atmosphere: Chemistry and Physics of the Stratosphere and Mesosphere, Springer Dordrecht, Dordrecht, 646 pp., doi: 10.1007/1-4020-3824-0, 2005.

Brohede, S. M., Haley, C. S., McLinden, C. A., Sioris, C. E., Murtagh, D. P., Petelina, S. V., Llewellyn, E. J., Bazureau, A., Goutail, F., Randall, C. E., Lumpe, J. D., Taha, G., Thomasson, L. W., and Gordley, L. L.: Validation of Odin/OSIRIS stratospheric NO_2 profiles, Journal of Geophysical Research: Atmospheres, 112, doi: 10.1029/2006JD007586, 2007.

Brown, L. R., Gunson, M. R., Toth, R. A., Irion, F. W., Rinsland, C. P., and Goldman, A.: 1995 Atmospheric Trace Molecule Spectroscopy (ATMOS) linelist, Appl Opt, 35, 2828-2848, doi: 10.1364/AO.35.002828, 1996.

Camy-Peyret, C., Flaud, J. M., Laurent, J., and Stokes, G. M.: First infrared measurement of atmospheric NO_2 from the ground, Geophys Res Lett, 10, 35-38, doi: 10.1029/GL010i001p00035, 1983.

Cariolle, D.: The ozone budget in the stratosphere: Results of a one-dimensional photochemical model, Planet Space Sci, 31, 1033-1052, doi: 10.1016/0032-0633(83)90093-4, 1983.

Cisewski, M., Zawodny, J., Gasbarre, J., Eckman, R., Topiwala, N., Rodriguez-Alvarez, O., Cheek, D., and Hall, S.: The stratospheric aerosol and gas experiment (SAGE III) on the International Space Station (ISS) Mission, Sensors, Systems, and Next-Generation Satellites XVIII, 59-65,

Chu, W. P., Trepte, C. R., Veiga, R. E., Cisewski, M. S., and Taha, G.: SAGE III measurements, Earth Observing Systems VII, 457-464, doi: 10.1117/12.451515, 2002.

Coffey, M. T., Mankin, W. G., and Goldman, A.: Simultaneous spectroscopic determination of the latitudinal, seasonal, and diurnal variability of stratospheric N_2O, NO, NO_2, and HNO_3, Journal of Geophysical Research, 86, 7331-7341, doi: 10.1029/JC086iC08p07331, 1981.

Cohen, R. C. and Murphy, J. G.: Photochemistry of NO_2 in Earth's stratosphere: constraints from observations, Chem Rev, 103, 4985-4998, doi: 10.1021/cr020647x, 2003.

Crutzen, P. J.: The influence of nitrogen oxides on the atmospheric ozone content, Quarterly Journal of the Royal Meteorological Society, 96, 320-325, doi: 10.1002/qj.49709640815, 1970.

Crutzen, P. J.: The Role of NO and NO_2 in the Chemistry of the Troposphere and Stratosphere, Annual Review of Earth and Planetary Sciences, 7, 443-472, doi: 10.1146/annurev.ea.07.050179.002303, 1979.

Dimitropoulou, E., Hendrick, F., Pinardi, G., Friedrich, M. M., Merlaud, A., Tack, F., De Longueville, H., Fayt, C., Hermans, C., Laffineur, Q., Fierens, F., and Van Roozendael, M.: Validation of TROPOMI tropospheric NO_2 columns using dual-scan multi-axis differential optical absorption spectroscopy (MAX-DOAS) measurements in Uccle, Brussels, Atmos. Meas. Tech., 13, 5165-5191, doi: 10.5194/amt-13-5165-2020, 2020.

Dubé, K., Randel, W., Bourassa, A., Zawada, D., McLinden, C., and Degenstein, D.: Trends and Variability in Stratospheric NO_x Derived From Merged SAGE II and OSIRIS Satellite Observations, Journal of Geophysical Research: Atmospheres, 125, doi: 10.1029/2019jd031798, 2020.

Dubé, K., Bourassa, A., Zawada, D., Degenstein, D., Damadeo, R., Flittner, D., and Randel, W.: Accounting for the photochemical variation in stratospheric NO_2 in the SAGE III/ISS solar occultation retrieval, Atmospheric Measurement Techniques, 14, 557-566, doi: 10.5194/amt-14-557-2021, 2021.

Fischer, H.: Remote Sensing of Atmospheric Trace Gases, Interdisciplinary Science Reviews, 18, 185-191, doi: 10.1179/isr.1993.18.3.185, 1993.

Flaud, J. M., Camy-Peyret, C., Brault, J. W., Rinsland, C. P., and Cariolle, D.: Nighttime and daytime variation of atmospheric NO from ground-based infrared measurements, Geophys Res Lett, 15, 261-264, doi: 10.1029/GL015i003p00261, 1988.

Funke, B., López-Puertas, M., von Clarmann, T., Stiller, G. P., Fischer, H., Glatthor, N., Grabowski, U., Höpfner, M., Kellmann, S., Kiefer, M., Linden, A., Mengistu Tsidu, G., Milz, M., Steck, T., and Wang, D. Y.: Retrieval of stratospheric NO_x from 5.3 and 6.2 μm nonlocal thermodynamic equilibrium emissions measured by Michelson Interferometer for Passive Atmospheric Sounding (MIPAS) on Envisat, Journal of Geophysical Research: Atmospheres, 110, doi: 10.1029/2004jd005225, 2005.

Fussen, D., Vanhellemont, F., Dodion, J., Bingen, C., Walker, K. A., Boone, C. D., McLeod, S. D., and Bernath, P. F.: Initial intercomparison of ozone and nitrogen dioxide number density profiles retrieved by the ACE-FTS and GOMOS occultation experiments, Geophys Res Lett, 32, doi: 10.1029/2005gl022468, 2005.

Godin-Beekmann, S.: Spatial observation of the ozone layer, Comptes Rendus Geoscience, 342, 339-348, doi: 10.1016/j.crte.2009.10.012, 2010.

Gordon, I. E., Rothman, L. S., Hargreaves, R. J., Hashemi, R., Karlovets, E. V., Skinner, F. M., Conway, E. K., Hill, C., Kochanov, R. V., Tan, Y., Wcisło, P., Finenko, A. A., Nelson, K., Bernath, P. F., Birk, M., Boudon, V., Campargue, A., Chance, K. V., Coustenis, A., Drouin, B. J., Flaud, J. M., Gamache, R. R., Hodges, J. T., Jacquemart, D., Mlawer, E. J., Nikitin, A. V., Perevalov, V. I., Rotger, M., Tennyson, J., Toon, G. C., Tran, H., Tyuterev, V. G., Adkins, E. M., Baker, A., Barbe, A., Canè, E., Császár, A. G., Dudaryonok, A., Egorov, O., Fleisher, A. J., Fleurbaey, H., Foltynowicz, A., Furtenbacher, T., Harrison, J. J., Hartmann, J. M., Horneman, V. M., Huang, X., Karman, T., Karns, J., Kassi, S., Kleiner, I., Kofman, V., Kwabia–Tchana, F., Lavrentieva, N. N., Lee, T. J., Long, D. A., Lukashevskaya, A. A., Lyulin, O. M., Makhnev, V. Y., Matt, W., Massie, S. T., Melosso, M., Mikhailenko, S. N., Mondelain, D., Müller, H. S. P., Naumenko, O. V., Perrin, A., Polyansky, O. L., Raddaoui, E., Raston, P. L., Reed, Z. D., Rey, M., Richard, C., Tóbiás, R., Sadiek, I., Schwenke, D. W., Starikova, E., Sung, K., Tamassia, F., Tashkun, S. A., Vander Auwera, J., Vasilenko, I. A., Vigasin, A. A., Villanueva, G. L., Vispoel, B., Wagner, G., Yachmenev, A., and Yurchenko, S. N.: The HITRAN2020 molecular spectroscopic database, Journal of Quantitative Spectroscopy and Radiative Transfer, 277, 107949, doi: 10.1016/j.jqsrt.2021.107949, 2022.

Grewe, V., Brunner, D., Dameris, M., Grenfell, J. L., Hein, R., Shindell, D., and Staehelin, J.: Origin and variability of upper tropospheric nitrogen oxides and ozone at northern mid-latitudes, Atmospheric Environment, 35, 3421-3433, doi: 10.1016/s1352-2310(01)00134-0, 2001.

Griffin, D., McLinden, C. A., Boersma, F., Bourassa, A., Dammers, E., Degenstein, D., Eskes, H., Fehr, L., Fioletov, V., Hayden, K., Kharol, S. K., Li, S. M., Makar, P., Martin, R. V., Mihele, C., Mittermeier, R. L., Krotkov, N., Sneep, M., Lamsal, L. N., Ter Linden, M., van Geffen, J., Veefkind, P., Wolde, M., and Zhao, X.: High resolution mapping of nitrogen dioxide with TROPOMI: First results and validation over the Canadian oil sands, Geophys Res Lett, 46, 1049-1060, doi: 10.1029/2018GL081095, 2019.

Haley, C. S., Brohede, S. M., Sioris, C. E., Griffioen, E., Murtagh, D. P., McDade, I. C., Eriksson, P., Llewellyn, E. J., Bazureau, A., and Goutail, F.: Retrieval of stratospheric O3 and NO2 profiles from Odin Optical Spectrograph and Infrared Imager System (OSIRIS) limb-scattered sunlight measurements, Journal of Geophysical Research: Atmospheres, 109, doi: 10.1029/2004jd004588, 2004.

Hanst, P. L., Wong, N. W., and Bragin, J.: A long-path infra-red study of Los Angeles smog, Atmospheric Environment, 16, 969-981, 1982.

Hase, F., Hannigan, J. W., Coffey, M. T., Goldman, A., Höpfner, M., Jones, N. B., Rinsland, C. P., and Wood, S. W.: Intercomparison of retrieval codes used for the analysis of high-resolution, ground-based FTIR measurements, Journal of Quantitative Spectroscopy and Radiative Transfer, 87, 25-52, doi: 10.1016/j.jqsrt.2003.12.008, 2004.

Hendrick, F., Mahieu, E., Bodeker, G. E., Boersma, K. F., Chipperfield, M. P., De Mazière, M., De Smedt, I., Demoulin, P., Fayt, C., Hermans, C., Kreher, K., Lejeune, B., Pinardi, G., Servais, C., Stübi, R., van der A, R., Vernier, J. P., and Van Roozendael, M.: Analysis of stratospheric NO2 trends above Jungfraujoch using ground-based UV-visible, FTIR, and satellite nadir observations, Atmospheric Chemistry and Physics, 12, 8851-8864, doi: 10.5194/acp-12-8851-2012, 2012.

Heue, K. P., Richter, A., Bruns, M., Burrows, J. P., v. Friedeburg, C., Platt, U., Pundt, I., Wang, P., and Wagner, T.: Validation of SCIAMACHY tropospheric NO2-columns with AMAXDOAS measurements, Atmospheric Chemistry and Physics, 5, 1039-1051, doi: 10.5194/acp-5-1039-2005, 2005.

Hönninger, G., von Friedeburg, C., and Platt, U.: Multi axis differential optical absorption spectroscopy (MAX-DOAS), Atmos. Chem. Phys., 4, 231-254, doi: 10.5194/acp-4-231-2004, 2004.

Jaeglé, L., Webster, C. R., May, R. D., Fahey, D. W., Woodbridge, E. L., Keim, E. R., Gao, R. S., Proffitt, M. H., Stimpfle, R. M., Salawitch, R. J., Wofsy, S. C., and Pfister, L.: In situ measurements of the NO2/NO ratio for testing atmospheric photochemical models, Geophys Res Lett, 21, 2555-2558, doi: 10.1029/94gl02717, 1994.

Johnston, H. S.: Atmospheric ozone, Annu Rev Phys Chem, 43, 1-31, doi: 10.1146/annurev.pc.43.100192.000245, 1992.

Kerzenmacher, T., Wolff, M. A., Strong, K., Dupuy, E., Walker, K. A., Amekudzi, L. K., Batchelor, R. L., Bernath, P. F., Berthet, G., Blumenstock, T., Boone, C. D., Bramstedt, K., Brogniez, C., Brohede, S., Burrows, J. P., Catoire, V., Dodion, J., Drummond, J. R., Dufour, D. G., Funke, B., Fussen, D., Goutail, F., Griffith, D. W. T., Haley, C. S., Hendrick, F., Höpfner, M., Huret, N., Jones, N., Kar, J., Kramer, I., Llewellyn, E. J., López-Puertas, M., Manney, G., McElroy, C. T., McLinden, C. A., Melo, S., Mikuteit, S., Murtagh, D., Nichitiu, F., Notholt, J., Nowlan, C., Piccolo, C., Pommereau, J. P., Randall, C., Raspollini, P., Ridolfi, M., Richter, A., Schneider, M., Schrems, O., Silicani, M., Stiller, G. P., Taylor, J., Tétard, C., Toohey, M., Vanhellemont, F., Warneke, T., Zawodny, J. M., and Zou, J.: Validation of NO2 and NO from the Atmospheric Chemistry Experiment (ACE), Atmospheric Chemistry and Physics, 8, 5801-5841, doi: 10.5194/acp-8-5801-2008, 2008.

Lamarque, J.-F., Kinnison, D. E., Mills, M. J., Marsh, D. R., Calvo, N., and Polvani, L. M.: Climate Change from 1850 to 2005 Simulated in CESM1(WACCM), Journal of Climate, 26, 7372-7391, doi: 10.1175/jcli-d-12-00558.1, 2013.

Lary, D. J.: Catalytic destruction of stratospheric ozone, Journal of Geophysical Research: Atmospheres, 102, 21515-21526, doi: 10.1029/97jd00912, 1997.

Laughner, J., Andrews, A., Roche, S., Kiel, M., and Toon, G. C.: ginput v1.1.15: GGG2020 prior profile software, CaltechDATA, doi: 10.22002/D1.8974, 2022.

Li, K.-F., Khoury, R., Pongetti, T. J., Sander, S. P., Mills, F. P., and Yung, Y. L.: Diurnal variability of stratospheric column NO2 measured using direct solar and lunar spectra over Table Mountain, California (34.38° N), Atmospheric Measurement Techniques, 14, 7495-7510, doi: 10.5194/amt-14-7495-2021, 2021.

McLinden, C. A., Olsen, S. C., Hannegan, B., Wild, O., Prather, M. J., and Sundet, J.: Stratospheric ozone in 3-D models: A simple chemistry and the cross-tropopause flux, Journal of Geophysical Research: Atmospheres, 105, 14653-14665, doi: 10.1029/2000jd900124, 2000.

Murphy, D. M., Fahey, D. W., Proffitt, M. H., Liu, S. C., Chan, K. R., Eubank, C. S., Kawa, S. R., and Kelly, K. K.: Reactive nitrogen and its correlation with ozone in the lower stratosphere and upper troposphere, Journal of Geophysical Research: Atmospheres, 98, 8751-8773, doi: 10.1029/92jd00681, 1993.

Notholt, J., Meier, A., and Peil, S.: Total column densities of tropospheric and stratospheric trace gases in the undisturbed Arctic summer atmosphere, Journal of Atmospheric Chemistry, 20, 311-332, doi: 10.1007/bf00694500, 1995.

Nürnberg, P., Sussmann, R., and Rettinger, M.: Solar FTIR measurements of NOx vertical distributions: Part II) Experiment-based scaling factors describing the diurnal increase of stratospheric NOx, Atmos. Chem. Phys., 2023.

Platt, U. and Stutz, J.: Differential Absorption Spectroscopy, in: Differential Optical Absorption Spectroscopy: Principles and Applications, Physics of Earth and Space Environments, Springer Berlin Heidelberg, Berlin, Heidelberg, 135-174, doi: 10.1007/978-3-540-75776-4_6, 2008.

Pommereau, J. P. and Goutail, F.: Stratospheric O3 and NO2 observations at the southern polar circle in summer and fall 1988, Geophys Res Lett, 15, 895-897, doi: 10.1029/GL015i008p00895, 1988.

Ricaud, P., Baron, P., and de La Noë, J.: Quality assessment of ground-based microwave measurements of chlorine monoxide, ozone, and nitrogen dioxide from the NDSC radiometer at the Plateau de Bure, Annales Geophysicae, 22, 1903-1915, 2004.

Richter, A. and Burrows, J. P.: Tropospheric NO2 from GOME measurements, Advances in Space Research, 29, 1673-1683, doi: 10.1016/s0273-1177(02)00100-x, 2002.

515 Rinsland, C. P., Goldman, A., Murcray, F. J., Murcray, F. H., Blatherwick, R. D., and Murcray, D. G.: Infrared measurements of atmospheric gases above Mauna Loa, Hawaii, in February 1987, Journal of Geophysical Research, 93, 12607-12626, doi: 10.1029/JD093iD10p12607, 1988.

Rodgers, C. D.: Information content and optimisation of high spectral resolution remote measurements, Advances in Space Research, 21, 361-367, doi: 10.1016/s0273-1177(97)00915-0, 1998.

520 Rusch, D. W.: Satellite ultraviolet measurements of nitric oxide fluorescence with a diffusive transport model, Journal of Geophysical Research, 78, 5676-5686, doi: 10.1029/JA078i025p05676, 1973.

Sierk, B., Richter, A., Rozanov, A., Von Savigny, C., Schmoltner, A. M., Buchwitz, M., Bovensmann, H., and Burrows, J. P.: Retrieval and monitoring of atmospheric trace gas concentrations in nadir and limb geometry using the space-borne SCIAMACHY instrument, Environ Monit Assess, 120, 65-77, doi: 10.1007/s10661-005-9049-9, 2006.

525 Solomon, S., Russell III, J. M., and Gordley, L. L.: Observations of the diurnal variation of nitrogen dioxide in the stratosphere, Journal of Geophysical Research: Atmospheres, 91, 5455-5464, doi: 10.1029/JD091iD05p05455, 1986.

Solomon, S., Schmeltekopf, A. L., and Sanders, R. W.: On the interpretation of zenith sky absorption measurements, Journal of Geophysical Research, 92, 8311-8319, doi: 10.1029/JD092iD07p08311, 1987.

Strode, S. A., Taha, G., Oman, L. D., Damadeo, R., Flittner, D., Schoeberl, M., Sioris, C. E., and Stauffer, R.: SAGE III/ISS
530 ozone and NO_2 validation using diurnal scaling factors, Atmospheric Measurement Techniques, 15, 6145-6161, doi: 10.5194/amt-15-6145-2022, 2022.

Sussmann, R.: Ground-based Fourier transform spectrometry at the NDSC site Zugspitze: Geophysical products for satellite validation, Proceedings of the European Symposium on Atmospheric Measurements from Space, ESTEC, Noordwijk, The Netherlands, 18-22 Jan., WPP-161, 2, 661-664, 1999.

535 Sussmann, R. and Schäfer, K.: Infrared spectroscopy of tropospheric trace gases: combined analysis of horizontal and vertical column abundances, Appl. Opt., 36, 735-741, doi: 10.1364/AO.36.000735, 1997.

Sussmann, R., Stremme, W., Burrows, J. P., Richter, A., Seiler, W., and Rettinger, M.: Stratospheric and tropospheric NO_2 variability on the diurnal and annual scale: a combined retrieval from ENVISAT/SCIAMACHY and solar FTIR at the Permanent Ground-Truthing Facility Zugspitze/Garmisch, Atmospheric Chemistry and Physics, 5, 2657-2677, doi:
540 10.5194/acp-5-2657-2005, 2005.

Tack, F., Hendrick, F., Goutail, F., Fayt, C., Merlaud, A., Pinardi, G., Hermans, C., Pommereau, J. P., and Van Roozendael, M.: Tropospheric nitrogen dioxide column retrieval from ground-based zenith–sky DOAS observations, Atmospheric Measurement Techniques, 8, 2417-2435, doi: 10.5194/amt-8-2417-2015, 2015.

Tikhonov, A. N.: On the solution of ill-posed problems and the method of regularization, Dokl. Akad. Nauk SSSR, 151, 501-
545 504, 1963.

Tripp, J. T.: The UNEP montreal protocol: Industrialized and developing countries sharing the responsibility for protecting the stratospheric ozone layer, NYUJ Int'l L. & Pol., 20, 733, 1987.

van Geffen, J., Eskes, H., Compernolle, S., Pinardi, G., Verhoelst, T., Lambert, J.-C., Sneep, M., ter Linden, M., Ludewig, A., Boersma, K. F., and Veefkind, J. P.: Sentinel-5P TROPOMI NO_2 retrieval: impact of version v2.2 improvements and
550 comparisons with OMI and ground-based data, Atmospheric Measurement Techniques, 15, 2037-2060, doi: 10.5194/amt-15-2037-2022, 2022.

Vandaele, A. C., Fayt, C., Hendrick, F., Hermans, C., Humbled, F., Van Roozendael, M., Gil, M., Navarro, M., Puentedura, O., Yela, M., Braathen, G., Stebel, K., Tørnkvist, K., Johnston, P., Kreher, K., Goutail, F., Mieville, A., Pommereau, J.-P., Khaikine, S., Richter, A., Oetjen, H., Wittrock, F., Bugarski, S., Frieß, U., Pfeilsticker, K., Sinreich, R., Wagner, T., Corlett,
555 G., and Leigh, R.: An intercomparison campaign of ground-based UV-visible measurements of NO_2, BrO, and OClO slant columns: Methods of analysis and results for NO_2, Journal of Geophysical Research: Atmospheres, 110, doi: 10.1029/2004jd005423, 2005.

Verhoelst, T., Compernolle, S., Pinardi, G., Lambert, J.-C., Eskes, H. J., Eichmann, K.-U., Fjæraa, A. M., Granville, J., Niemeijer, S., Cede, A., Tiefengraber, M., Hendrick, F., Pazmiño, A., Bais, A., Bazureau, A., Boersma, K. F., Bognar, K.,
560 Dehn, A., Donner, S., Elokhov, A., Gebetsberger, M., Goutail, F., Grutter de la Mora, M., Gruzdev, A., Gratsea, M., Hansen, G. H., Irie, H., Jepsen, N., Kanaya, Y., Karagkiozidis, D., Kivi, R., Kreher, K., Levelt, P. F., Liu, C., Müller, M., Navarro Comas, M., Piters, A. J. M., Pommereau, J.-P., Portafaix, T., Prados-Roman, C., Puentedura, O., Querel, R., Remmers, J., Richter, A., Rimmer, J., Rivera Cárdenas, C., Saavedra de Miguel, L., Sinyakov, V. P., Stremme, W., Strong, K., Van Roozendael, M., Veefkind, J. P., Wagner, T., Wittrock, F., Yela González, M., and Zehner, C.: Ground-based validation of the
565 Copernicus Sentinel-5P TROPOMI NO_2 measurements with the NDACC ZSL-DOAS, MAX-DOAS and Pandonia global networks, Atmospheric Measurement Techniques, 14, 481-510, doi: 10.5194/amt-14-481-2021, 2021.

Virolainen, Y., Timofeyev, Y., Polyakov, A., Ionov, D., and Poberovsky, A.: Intercomparison of satellite and ground-based measurements of ozone, NO_2, HF, and HCl near Saint Petersburg, Russia, International Journal of Remote Sensing, 35, 5677-5697, doi: 10.1080/01431161.2014.945009, 2014.

570 Wang, S., Li, K.-F., Zhu, D., Sander, S. P., Yung, Y. L., Pazmino, A., and Querel, R.: Solar 11-Year Cycle Signal in Stratospheric Nitrogen Dioxide—Similarities and Discrepancies Between Model and NDACC Observations, Solar Physics, 295, 117, doi: 10.1007/s11207-020-01685-1, 2020.

Wetzel, G., Bracher, A., Funke, B., Goutail, F., Hendrick, F., Lambert, J. C., Mikuteit, S., Piccolo, C., Pirre, M., Bazureau, A., Belotti, C., Blumenstock, T., De Mazière, M., Fischer, H., Huret, N., Ionov, D., López-Puertas, M., Maucher, G., Oelhaf, H.,
575 Pommereau, J. P., Ruhnke, R., Sinnhuber, M., Stiller, G., Van Roozendael, M., and Zhang, G.: Validation of MIPAS-ENVISAT NO_2 operational data, Atmospheric Chemistry and Physics, 7, 3261-3284, doi: 10.5194/acp-7-3261-2007, 2007.

Wiacek, A., Jones, N. B., Strong, K., Taylor, J. R., Mittermeier, R. L., and Fast, H.: First detection of meso-thermospheric Nitric Oxide (NO) by ground-based FTIR solar absorption spectroscopy, Geophys Res Lett, 33, doi: 10.1029/2005gl024897, 2006.

580   World Health Organization. Regional Office for Europe: Health aspects of air pollution with particulate matter, ozone and nitrogen dioxide : report on a WHO working group, Bonn, Germany 13-15 January 2003, Copenhagen : WHO Regional Office for Europe, https://apps.who.int/iris/handle/10665/107478, 2003.

Yin, H., Sun, Y., Liu, C., Zhang, L., Lu, X., Wang, W., Shan, C., Hu, Q., Tian, Y., Zhang, C., Su, W., Zhang, H., Palm, M., Notholt, J., and Liu, J.: FTIR time series of stratospheric NO_2 over Hefei, China, and comparisons with OMI and GEOS-Chem
585   model data, Opt Express, 27, A1225-A1240, doi: 10.1364/OE.27.0A1225, 2019.

York, D., Evensen, N. M., Martínez, M. L., and Delgado, J. D. B.: Unified equations for the slope, intercept, and standard errors of the best straight line, American Journal of Physics, 72, 367-375, doi: 10.1119/1.1632486, 2004.

Zhou, M., Langerock, B., Vigouroux, C., Dils, B., Hermans, C., Kumps, N., Nan, W., Metzger, J.-M., Mahieu, E., Wang, T., Wang, P., and De Mazière, M.: Tropospheric and stratospheric NO retrieved from ground-based Fourier-transform infrared
590   (FTIR) measurements, Atmospheric Measurement Techniques, 14, 6233-6247, doi: 10.5194/amt-14-6233-2021, 2021.

Table 1. Results of Garmisch-Zugspitze diurnal increasing rate correlation analysis. The correlation coefficient r, r^2, and the calculated t-values from the linear regression with x- and y-error weighting and without. Significant correlation is achieved if the t-value exceeds the critical t-value t_{crit} for the given confidence level.

	Correlation coefficient r	r^2	t-value	t_{crit}(95 %)	Significant correlation within 95 % confidence?
with x- and y-error weighting			3.96	2.23	**yes**
	0.7899	0.6239			
no weighting			3.37	2.23	**yes**

Table 2. Results of NO-NO$_2$ diurnal increasing rate correlation analysis. The correlation coefficient r, r^2 and the calculated t-values from the linear regression with x- and y-error weighting and without weighting. Significant correlation is achieved if the t-value exceeds the critical t-value t_{crit} for the given confidence level.

	Correlation coefficient r	r^2	t-value	t_{crit}(95 %)	Significant correlation within 95 % confidence?
with x- and y-error weighting			0.83	2.23	No
	0.7798	0.6082			
no weighting			3.94	2.23	Yes
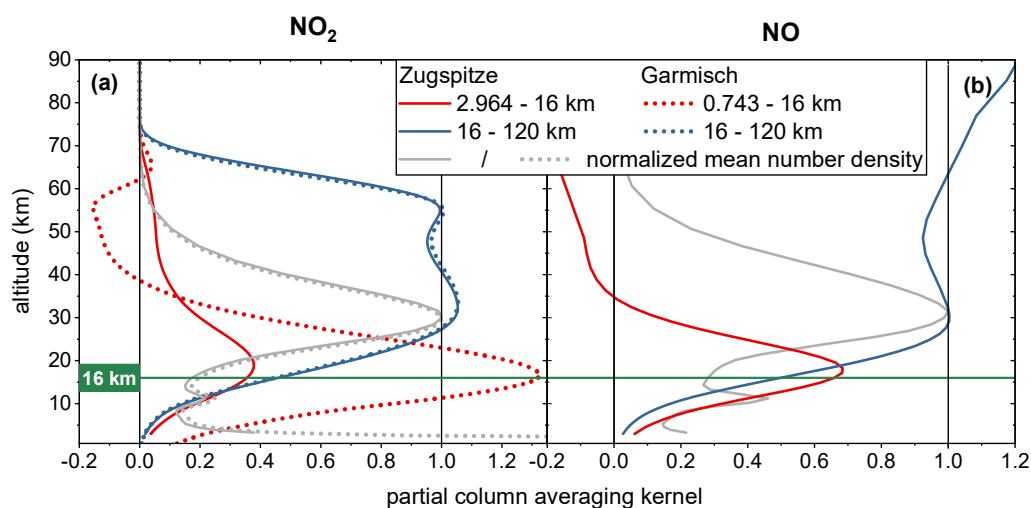
Figure 1. Retrieved partial column averaging kernels for below 16 km altitude (red lines) and above 16 km altitude (blue lines) of (a) NO$_2$ measured at Zugspitze (continuous lines) and Garmisch (dotted lines) and (b) NO measured at Zugspitze plotted in dependence of the altitude. Additionally, the respective normalized mean number density is shown in dependence of the altitude (gray lines). The green line indicates the splitting altitude 16 km.
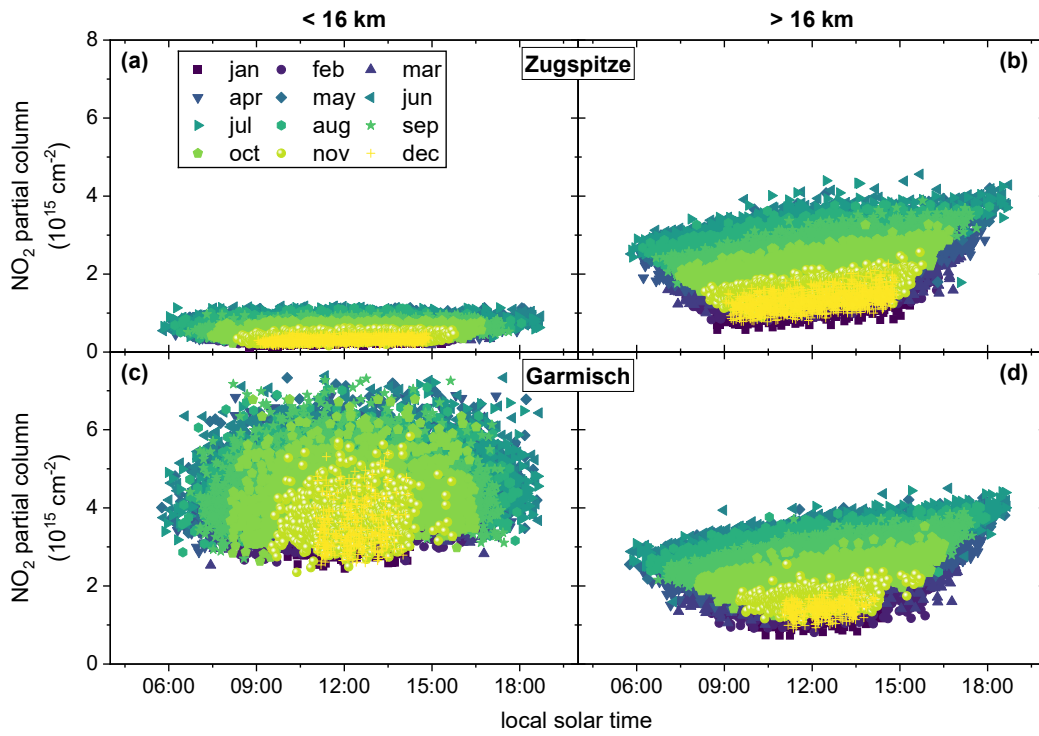
Figure 2. Retrieved pollution filtered NO$_2$ partial columns for every month below (a) and above (b) 16 km altitude measured at Zugspitze and below (c) and above (d) 16 km altitude measured at Garmisch in dependence of the local solar time (blue to yellow symbols from January to December, see legend).

610
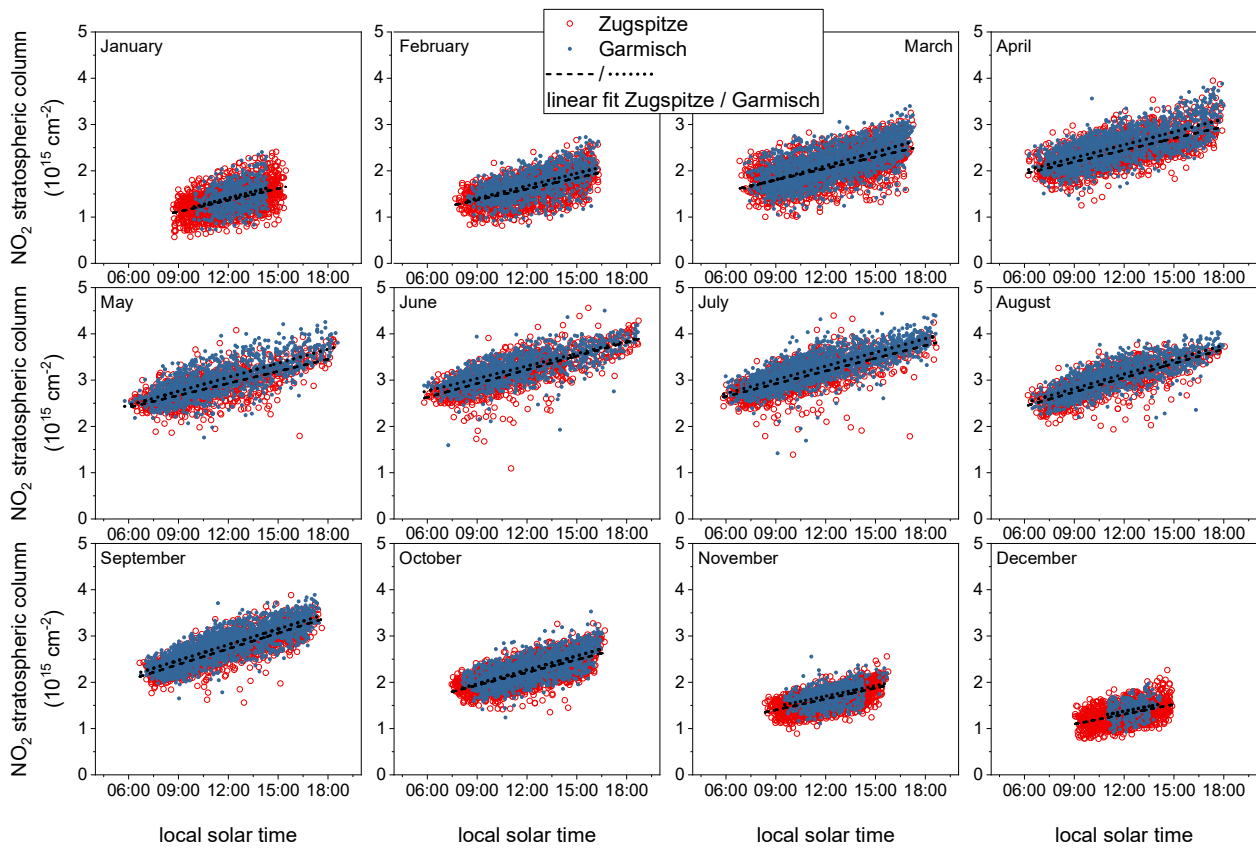
Figure 3. Retrieved pollution filtered NO$_2$ stratospheric columns (> 16 km) above Zugspitze (red open symbols) and Garmisch (blue closed symbols) for every month in dependence of the local solar time and linear fit between over the whole data range (black dashed and dotted lines for Zugspitze and Garmisch, respectively).

615
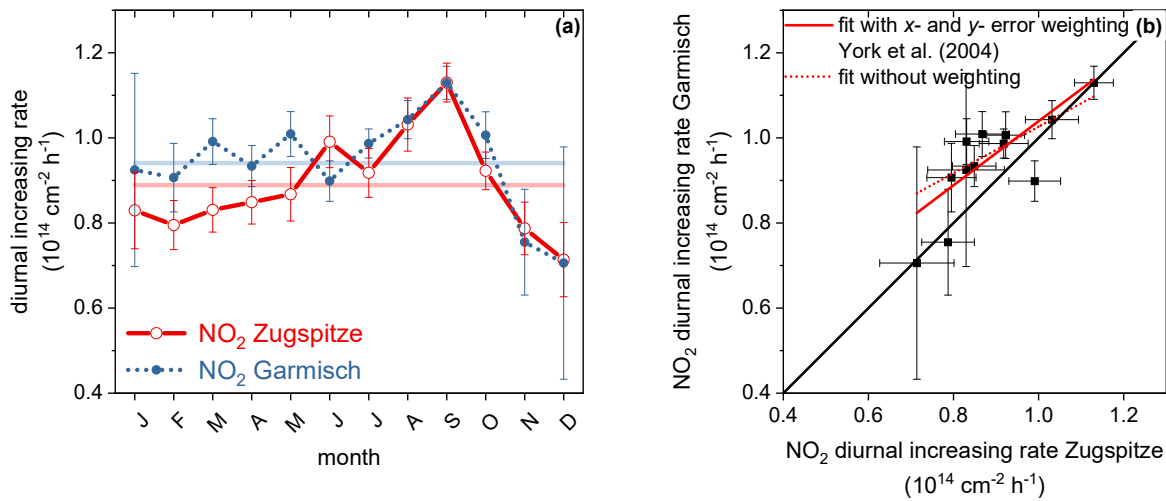
Figure 4. NO₂ diurnal increasing rates measured at Zugspitze and Garmisch. The error bars are ±2·σ (standard deviation) from the linear fit. (a) Data for Zugspitze (red open symbols) and Garmisch (blue closed symbols) in dependence of the month. The lines are guides to the eye only. (b) Scatter plot of the data measured at Garmisch against the data measured at Zugspitze (black data points). Additionally, the linear regression with *x*- and *y*-error weighting with the method of York et al (2004) (red continuous line) and without weighting (red dotted line) is shown. The 1:1 line is given in black.
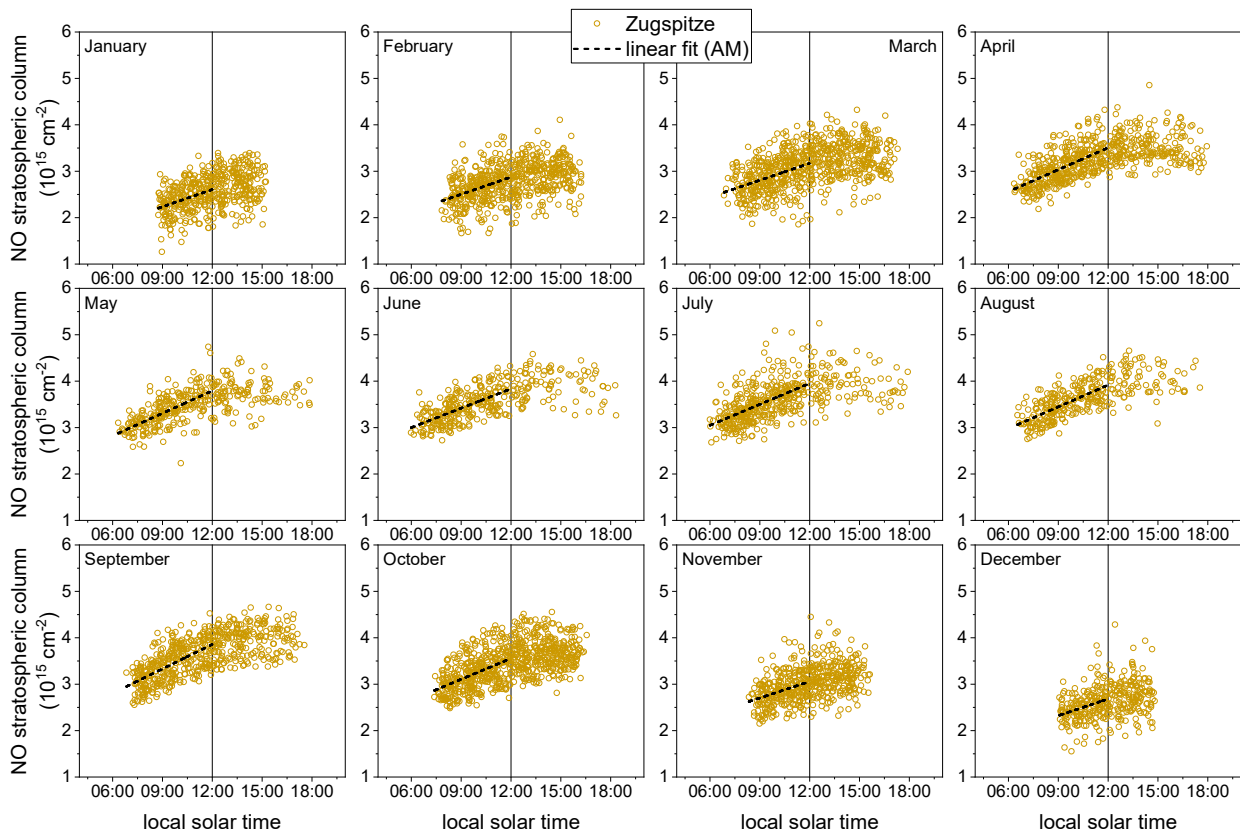
Figure 5. Retrieved pollution filtered NO stratospheric columns (> 16 km) above Zugspitze (yellow symbols) for every month in dependence of the local solar time and linear fit before local solar noon (black dashed line).
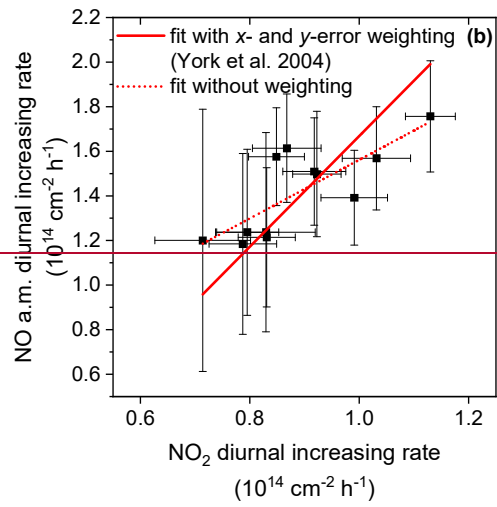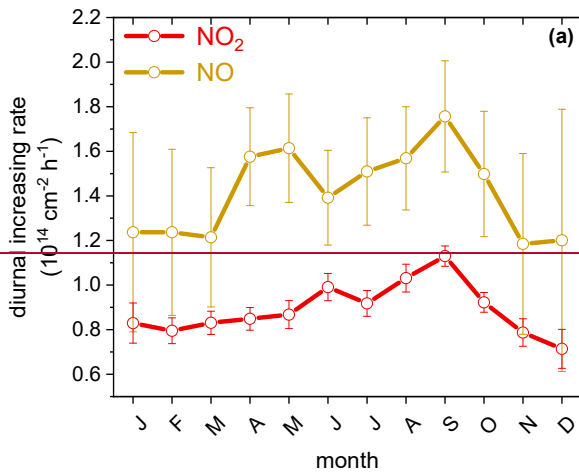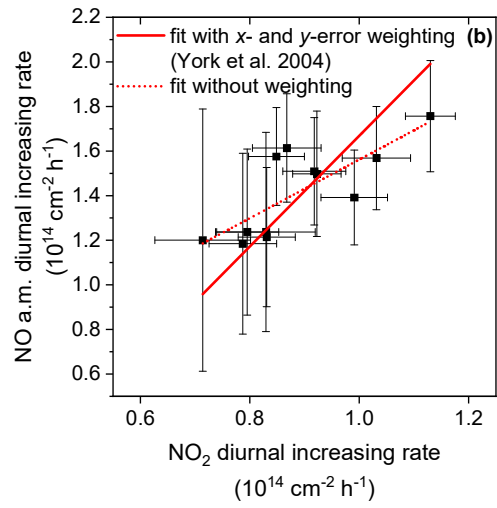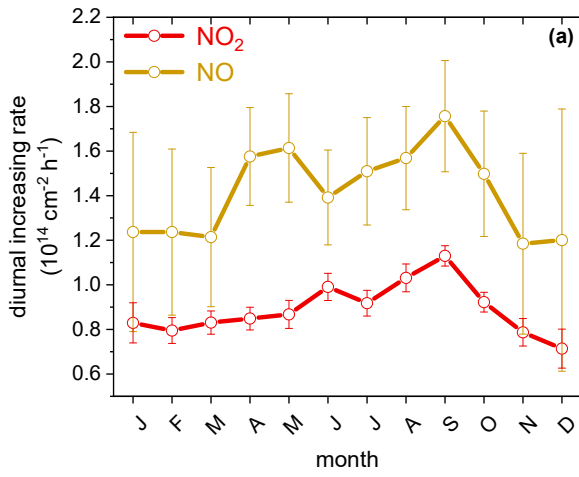
Figure 6. NO₂ diurnal increasing rates and NO a.m. diurnal increasing rates measured at Zugspitze. The error bars are ±2·σ (standard deviation) from the linear fit. (a) Data for NO₂ (red symbols) and NO (yellow symbols) in dependence of the month. The lines are guides to the eye only. (b) Scatter plot of the NO data against the NO₂ data both measured at Zugspitze (black data points). Additionally, the linear regression with *x*- and *y*-error weighting with the method of York et al. (2004) (red continuous line) and without weighting (red dotted line) is shown.